Applied Catalysis B: Environmental 132–133 (2013) 237–244

Contents lists available at SciVerse ScienceDirect

Applied Catalysis B: Environmental

journal homepage: www.elsevier.com/locate/apcatb

Nanostructure catalysts prepared by multi-sputtering deposition process for enhanced methanol electrooxidation reaction

Kyung-Won Park[a,*], Young-Woo Lee[a], Yung-Eun Sung[b,**]

[a] Department of Chemical Engineering, Soongsil University, Seoul 156743, Republic of Korea
[b] World Class University (WCU) Program of Chemical Convergence for Energy & Environment (C_2E_2), School of Chemical and Biological Engineering, College of Engineering, Seoul National University (SNU), Seoul 151742, Republic of Korea

ARTICLE INFO

Article history:
Received 2 August 2012
Received in revised form 6 November 2012
Accepted 28 November 2012
Available online 7 December 2012

Keywords:
Electrocatalyst
Direct methanol fuel cells
Size-control
Composition-control
Sputtering deposition process

ABSTRACT

We report size and/or composition-controlled nanostructure catalysts for direct methanol fuel cells fabricated by means of multi-sputtering deposition process. The size-controlled Pt nanophases ranging from 0.62 ± 0.14 nm to 3.07 ± 0.34 nm in average size with narrow size distribution are fabricated as a function of sputtering power ratio of targets. The composition-controlled PtRu alloy nanophases deposited at different RF power ratio of Pt and Ru targets with the same power of WO_3 target exhibit varied atomic percentages of PtRu, i.e. (79.8:21.2), (62.2:37.8) and (37.6:62.4). Furthermore, the PtRu nanophases deposited at a constant RF power ratio of Pt and Ru targets with different power of WO_3 target show controlled average sizes such as 3.62 ± 0.15 nm, 1.86 ± 0.23 nm, and 1.20 ± 0.22 nm with the same compositions. The specific maximum power density of the nanostructure catalyst ($\sim 100\ W\ g^{-1}$) is superior to that of the conventional nanostructure catalyst ($\sim 37\ W\ g^{-1}$), representing that the nanostructure catalyst has an excellent electrode structure for methanol electrooxidation as compared to the conventional catalyst.

1. Introduction

Electronic, chemical, magnetic, and optical properties of nanostructured materials are extremely different from those of bulk materials depending on size, shape, and composition [1–4]. In particular, since catalytic reaction process depends on the size of nanoparticles, synthesis of well size-controlled nanoparticles is crucial for effective catalysis study and catalysts for use in fuel cells [5–7]. Many studies on colloidal bulk particles have focused on the control of particle sizes and have been related to catalytic activity as a function of catalyst size [8,9].

Recently, the miniaturization of polymer electrolyte membrane fuel cells as a power source for small digital devices to microelectromechanical systems has been the subject of intense study [10–12]. The power sources for these applications should be small-sized for on chip or integration as well as have sufficiently available capability to operate the intended devices. Accordingly, electrodes for such miniaturized fuel cells should be considered and fabricated from point of view in both nanostructures for catalysis and thin-film formation for integration with other devices. The electrodes for conventional direct methanol fuel cells (DMFCs) based on bulk properties of catalysts commonly consist of more than two phases such as nanosized noble metals i.e. Pt, PtRu and porous materials i.e. carbon or porous oxides as an assistant or support [13–18].

However, conventional physical deposition methods have difficulty in providing the two-phase electrodes containing nanometallic phases as catalysts and porous oxides as supports, besides, possessing individual properties of each material. The conventional sputtering techniques with one sputtering target of a two phase mixed material or small chips of 2nd phase on the target of 1st phase might not be utilized to form size-controlled thin-film electrodes with various compositions keeping the individual properties of each material. Herein, we suggest multi-sputtering deposition (MSD) method with individual gun of metal and oxide targets in order to fabricate and design nanostructure catalysts containing size-controlled Pt or PtRu nanophases in porous material.

The size distribution of the catalysts was characterized by field-emission transmission electron microscopy (FE-TEM) Energy dispersive X-ray (EDX) analysis of the catalysts was performed on a FE-TEM (Tecnai G2 F30 system). The relative composition of Pt and Ru present in the catalysts was determined by Rutherford backscattering spectrometry (RBS). To evaluate the electrochemical properties of the catalysts, cyclic voltammograms (CVs) and current-potential curves were obtained using a three-electrode electrochemical system. The performance of the unit cell was evaluated using a computer-controlled electronic load.

* Corresponding author. Tel.: +82 2 820 0613; fax: +82 2 812 5378.
** Corresponding author.
E-mail addresses: kwpark@ssu.ac.kr (K.-W. Park), ysung@snu.ac.kr (Y.-E. Sung).

0926-3373/$ – see front matter © 2012 Elsevier B.V. All rights reserved.
http://dx.doi.org/10.1016/j.apcatb.2012.11.044

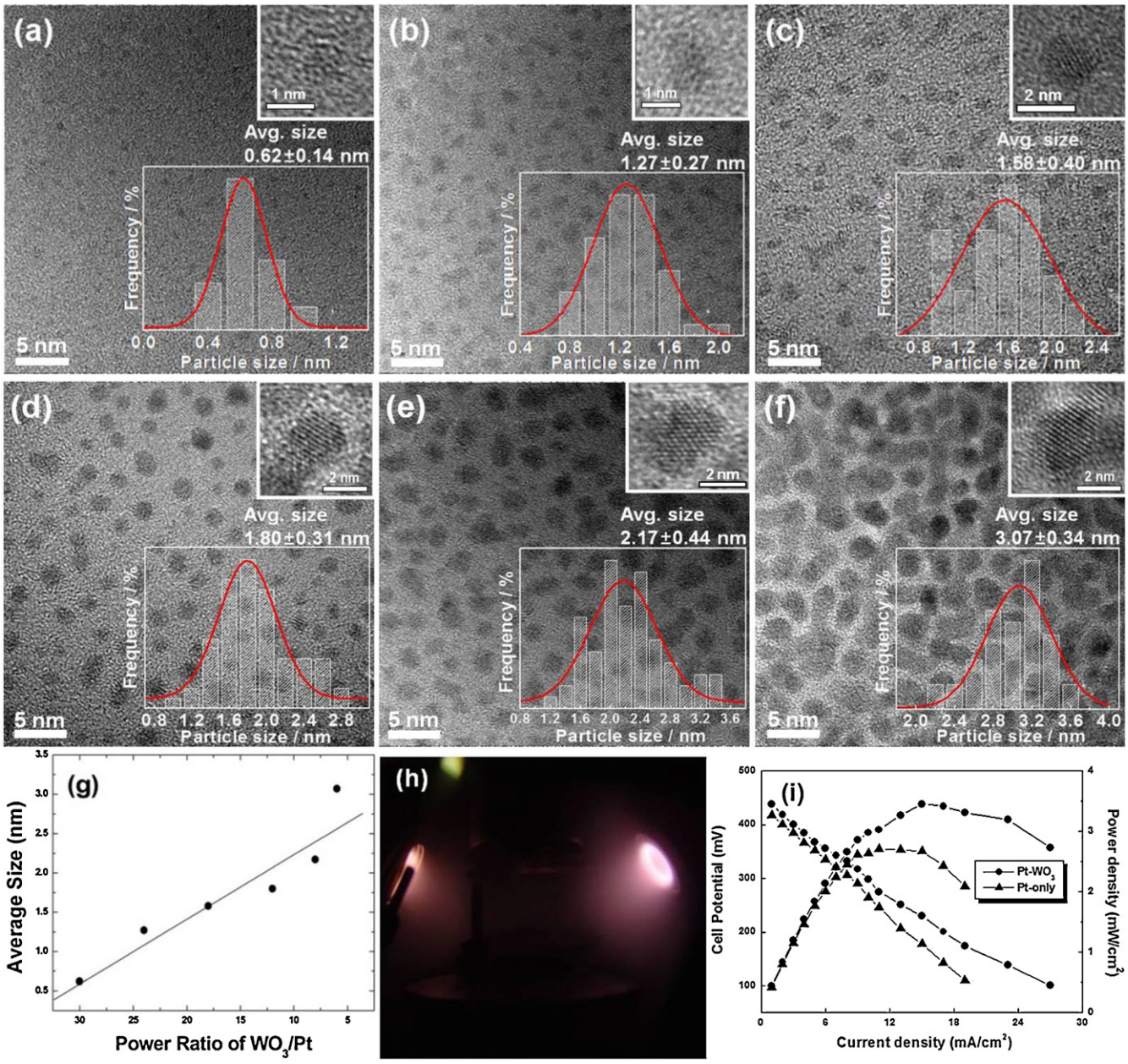

Fig. 1. TEM Images and size distributions of Pt–WO_3 nanostructure catalysts prepared as a function of power ratio (WO_3/Pt) of (a) 30, (b) 24, (c) 18, (d) 12, (e) 8, (f) 6 in the MSD system. (g) A plot of average size of Pt nanophases versus sputtering power ratio of targets. (h) Photo image of actual deposition process in the MSD system to fabricate the nanostructure catalysts. (i) Characteristic curves of DMFCs measured at 25 °C using Pt–WO_3 and Pt-only as an anode and Pt black powders as cathode catalysts.

2. Experimental

2.1. Fabrication of Pt nanostructure catalysts

Pt nanostructure catalysts were grown using radio frequency (RF) magnetron sputtering system with multi-sputtering targets. Indium tin oxides-coated transparent glasses (ITO, Samsung Corning Co., Ltd.) were used as substrate. Pt and WO_3 were used as the target materials. The base pressure was less than 5×10^{-6} Torr and working pressure was 1.1×10^{-2} Torr for all examined. Sputtering was carried out under Ar gas atmosphere at 30 SCCM at room temperature. The samples were sputter-deposited for 2 min at the RF powers of 10 W and 60–300 W of Pt and WO_3 target, respectively.

2.2. Fabrication of PtRu nanostructure catalysts

PtRu nanostructure catalysts were also prepared using RF magnetron sputtering system under an atmosphere of inert Ar gas at room temperature. In order to control PtRu alloy nanophases, the RF power of the Pt, Ru, and WO_3 sputtering targets were individually manipulated. For electrochemical analysis, the ITO-coated transparent glasses and teflonized carbon paper (Toray, TGPH-090) were used as substrates. The different composition of the same-sized PtRu alloy nanophases was modulated by the RF power of metal targets at constant powers of WO_3 target. The size of PtRu alloy nanophases with the same compositions was controlled by the RF power of WO_3 target at constant powers of metal targets.

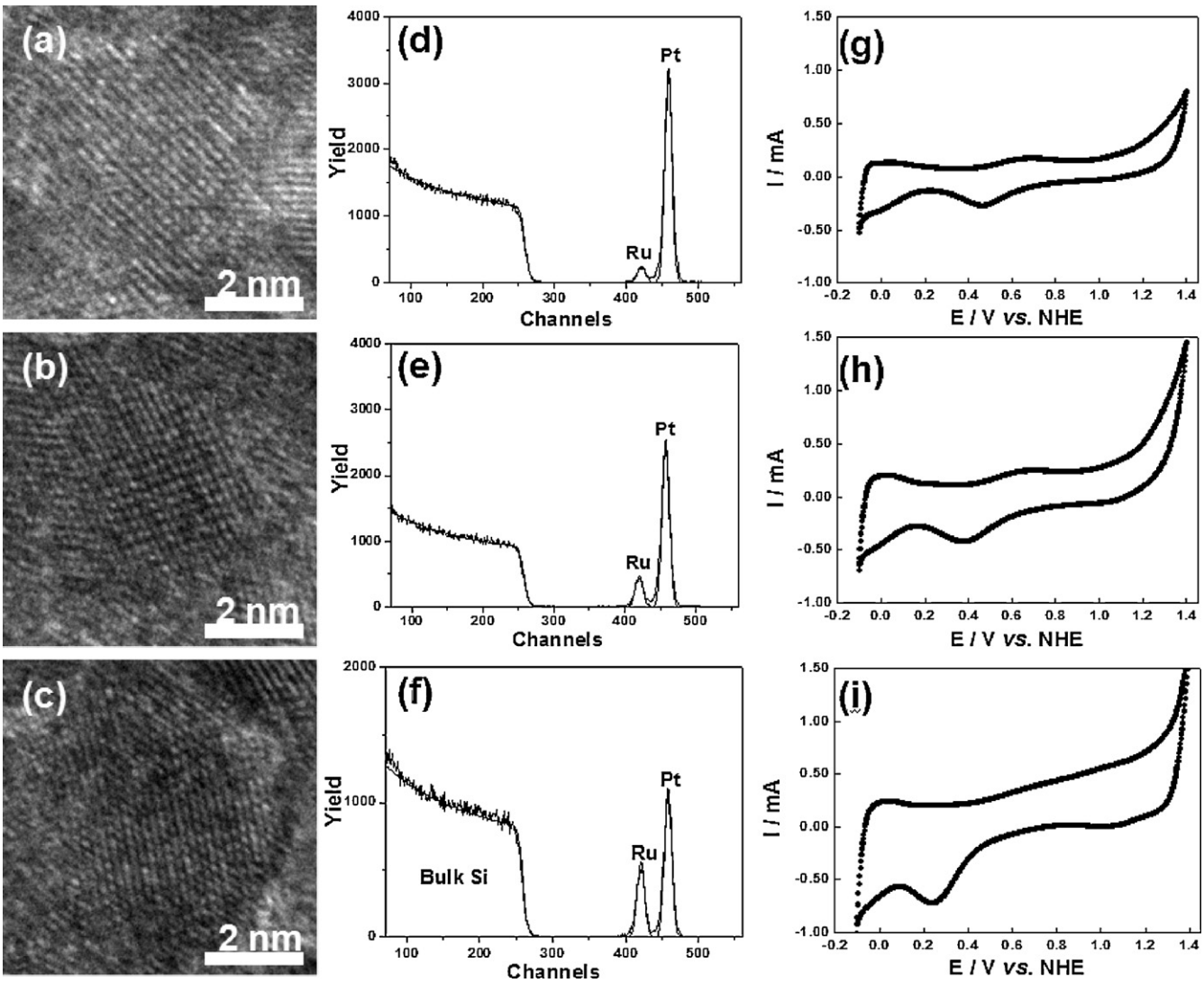

Fig. 2. TEM images of nanostructure catalysts fabricated with the RF powers of (a) 20 and 80 W, (b) 20 and 100 W, and (c) 20 and 120 W of Pt and Ru targets at a constant power (120 W) of WO_3. RBS spectra ((d)–(f)) and typical electrochemical characteristic curves ((g)–(i)) of the nanostructure catalysts.

2.3. Structure analysis of nanostructure catalysts

The size distribution of the catalysts was characterized by field-emission transmission electron microscopy (FE–TEM) using a Tecnai G2 F30 system operating at 300 kV. TEM samples were prepared by depositing on a carbon-coated copper grid. Energy dispersive X-ray (EDX) analysis of the catalysts was performed on a FE–TEM (Tecnai G2 F30 system). The relative composition of Pt and Ru present in the catalysts deposited by RF magnetron sputtering is determined by Rutherford backscattering spectrometry (RBS, NEC 3SDH) using a beam of He^+ ions with an energy of 2.243 MeV on the surface of the sample and by analyzing the energy spectrum of the backscattered ions in a high vacuum chamber ($<10^{-6}$ Torr). Backscattered ions were collected at an angle of 165° with a solid-state detector. Spectra were analyzed by simulation software of Hypra (Charls Evans & Associates) yielding the elemental composition of catalysts.

2.4. Electrochemical analysis of nanostructure catalysts

To evaluate the electrochemical properties of the catalysts, cyclic voltammograms (CVs) and current–potential curves were obtained using a three-electrode electrochemical system consisting of a deposited electrode, Pt wire, and Ag/AgCl as the working, counter, and reference electrode, respectively, at 25 °C. The solutions of 0.5 M H_2SO_4 and 2.0 M CH_3OH + 0.5 M H_2SO_4 were stirred constantly and purged with argon gas. For a membrane-electrode-assembly (MEA) of DMFC, the anode of 2 mg of PtRu /cm^2 (Johnson-Matthey Co.) or PtRu catalyst sputtered and cathode of 5 mg of Pt black, /cm^2 (Johnson-Matthey Co.) catalyst layers were formed on teflonized carbon paper substrates. The inks for catalyst layers prepared using the appropriate weight percent of Nafion® ionomer solution (Aldrich Co.) and catalyst powders. The MEA for unit cell tests were fabricated by pressing as prepared cathode and anode layers onto both sides of a pre-treated Nafion® 117 electrolyte membrane at 110 °C and 800 psi for 3 min. The performance of the unit cell with a 2 cm^2 cross-sectional area was evaluated using a computer-controlled electronic load (CNLPEM005-01, CNL Energy Co.). Both fuel and oxidant flow paths were machined into graphite block end plates, which also served as current collectors. A 2 M methanol solution with a flow rate of 1 cc min^{-1} was supplied by a Masterflex liquid micro-pump and dry O_2 flow was regulated at 500 cc min^{-1} using a flow meter.

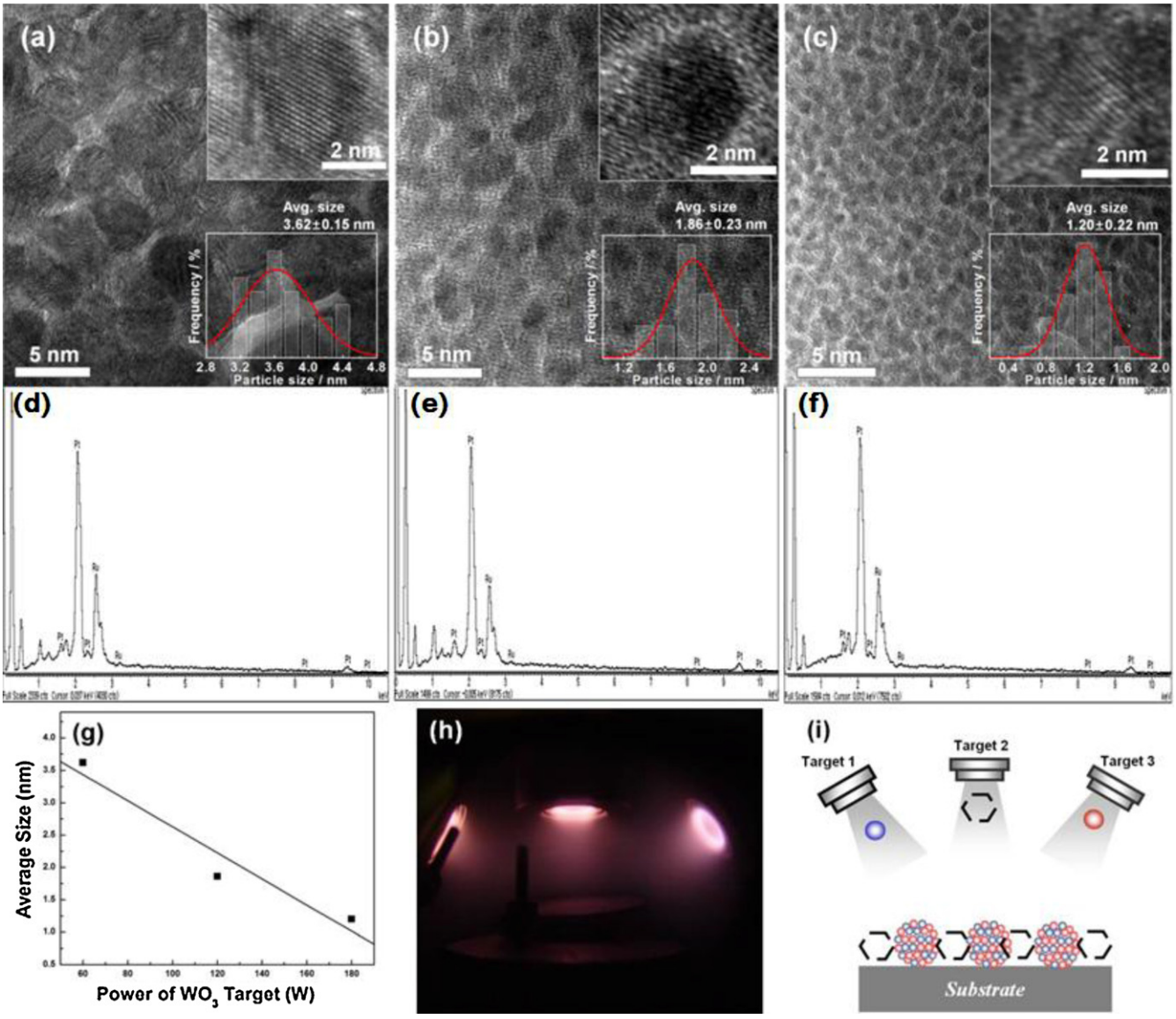

Fig. 3. TEM Images, size distributions, and EDX spectra of nanostructure catalysts fabricated at RF sputtering powers of 20 (Pt) and 100 (Ru) W and different WO_3 target powers of 60 ((a) and (d)), 120 ((b) and (e)), and 180 W ((c) and (f)). (g) A plot of average size of PtRu nanophases versus sputtering powers of WO_3 target. (h) Photo image and (i) schematic representation of deposition process in the MSD system to fabricate the nanostructure catalysts.

3. Results and discussion

Fig. 1 shows FE–TEM images of nanostructured catalysts prepared by controlling power ratio of sputtering gun of Pt metal and WO_3 target in RF magnetron sputtering system with multi-sputtering targets. In the TEM images, Pt nanophases are represented as dark image while tungsten oxides are represented as relatively white image. The interesting configuration of Pt–WO_3 nanostructure catalysts (Pt–WO_3) formed by MSD method is the phase separation between metallic Pt and oxidative WO_3 without any solid solution. In general, metals have high surface energies, i.e. Pt (2.475 J m^{-2}) and Ru (3.050 J m^{-2}) while oxides have low surface energies, i.e. WO_3 (0.1 J m^{-2}) [19,20]. The surface energy can determine whether one material wets another. This suggests that during deposition process in the MSD system, Pt having high surface energy might tend to form nanophases in tungsten oxide having low-surface-energy. In reality, it is considered that according to difference of surface energy between Pt and WO_3, nanosized Pt is spontaneously formed with WO_3 as matrix. Accordingly, the whole as-deposited catalysts show nanocomposite structure consisting of Pt metallic nanophase and tungsten oxide phase. Since the Pt nanophases are embedded into the tungsten oxide matrix forming a clear interface between Pt and WO_3, the interface can enhance the activity of the Pt catalysts due to the spillover effect of WO_3. As shown in the Fig. 1(a)–(f), the average size of Pt nanophases as a function of sputtering power ratio of targets, corresponds to ca. 0.62 ± 0.14, 1.27 ± 0.27, 1.58 ± 0.40, 1.80 ± 0.31, 2.17 ± 0.44 and 3.07 ± 0.34 nm in average size, respectively, with narrow size distribution. Furthermore, the (1 1 1) lattice of Pt metallic phases in the whole catalysts means very clear evidence of excellent crystallinity of the nanostructure catalysts. As indicated in Fig. 1(g) and (h), it is noticeable that the size of Pt nanophases can be modulated by power ratio of sputtering guns as a simple experimental parameter. The electrooxidation of methanol as a fuel in the DMFCs occurs at the anode as the following equation [21–23]: $CH_3OH + H_2O \rightarrow 6H^+ + 6e^- + CO_2$. However, since the catalytic reaction rate, i.e. current density of methanol electrooxidation, is proportional to active surface area of Pt as an expensive catalyst, the small-sized Pt is a requisite for an excellent catalytic reaction in fuel cells and catalysis. Fig. 1(i) shows characteristic curves of DMFCs

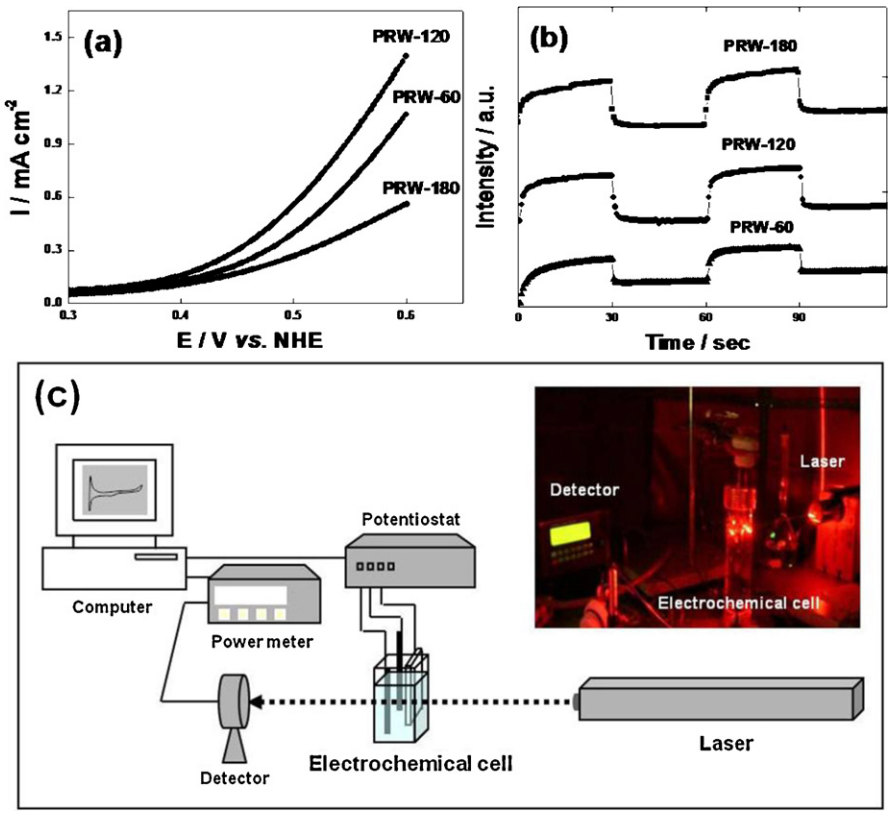

Fig. 4. (a) Characteristic curves of methanol electrooxidation current vs. applied potential of PRW catalysts in 2.0 M CH_3OH + 0.5 M H_2SO_4. (b) *In situ* transmittance curves of PRW catalysts with a pulse potential of −0.3/+0.5/−0.3/+0.5 V at an interval of 30 s in 2.0 M CH_3OH + 0.5 M H_2SO_4. (c) Schematic representation of *in situ* photo-electrochemical measurement using an electrochemical cell for methanol electrooxidation and an optical part consisting of a He–Ne laser (633 nm) as the light source with a power meter for the detection of optical signal modulation (The inset shows photo image of actual photo-electrochemical cell.).

measured at 25 °C using Pt–WO_3 formed by the MSD system and Pt-only formed using sputtering deposition without WO_3 target as anode catalysts, respectively, and Pt black powders as cathode catalysts. In the polarization curves, the Pt–WO_3 exhibits an improved activation polarization, i.e. high current density and maximum power density, representing highly efficient catalytic activity for methanol electrooxidation at the anode as compared to Pt-only anode. Furthermore, the crystallinity of Pt catalysts with different electrochemical properties can be fabricated by manipulating sputtering time at the power ratio of sputtering guns in the MSD system.

However, since pure Pt is readily poisoned by intermediates produced during methanol electrooxidation, Pt-based alloy or nanocomposite catalysts by alloying or mixing Pt with 2nd or 3rd elements need to be designed [24–28]. In general, the CO-poisoned Pt can be regenerated via the reaction of surface CO with oxygen species associated with an element such as Ru to yield CO_2 [29,30]. Furthermore, PtRu alloy with optimum ratio of Pt–Ru is extremely essential for enhanced methanol electrooxidation. We prepared nanocomposite electrodes by controlling power ratio of sputtering gun of Pt, Ru and WO_3 target (TEM images of Fig. 2(a)–(c)). The compositions of nanocomposite electrodes containing PtRu alloy nanophases surrounded by WO_3 matrix were controlled as a function of sputtering power of targets. The samples deposited at the RF powers of 20 and 80 W, 20 and 100 W, and 20 and 120 W of Pt and Ru targets with the same power (120 W) of WO_3 target exhibit varied atomic percentages (at.%) of PtRu, i.e. (79.8:21.2), (62.2:37.8) and (37.6:62.4), respectively (RBS spectra of Fig. 2(d)–(f)). The nanostructure catalysts show typical CVs depending on the surface composition of Pt and Ru (Fig. 2(g)–(i)). As the Ru component in the electrodes increases, the thickness of the double layer region at the potential range of 0.1–0.6 V increases due to the hydrophilic properties of Ru and the higher shift in potential for oxygen reduction due to the slow kinetics of Ru itself for oxygen reduction. This indicates that nanocomposite electrodes containing transition of Pt-based and Ru-based electrochemical properties can be fabricated using the MSD system.

It is well-known that the 50–60 at.% of Pt in the PtRu alloy catalysts is optimal for achieving excellent catalytic activity in methanol oxidation [31,32]. The nanocomposite electrode with 62.2 at.% of Pt was prepared using the RF powers of 20 and 100 W of Pt and Ru targets in the MSD system. The samples deposited at the RF powers of 20 and 100 W of Pt and Ru targets with 60, 120, and 180 W of WO_3 target (PRW-60, PRW-120, and PRW-180) exhibit controlled average sizes of PtRu nanophases such as 3.62 ± 0.15, 1.86 ± 0.23, and 1.20 ± 0.22 nm, respectively, (Fig. 3(a)–(c)) and the same compositions of PtRu. The nanostructure catalysts deposited at all the same RF powers of Pt and Ru targets and different RF powers of WO_3 target exhibit ~62 and ~38 at.% of Pt and Ru, respectively, as confirmed by EDX spectra of Fig. 3(d)–(f). Due to the phase separation between metallic phases and oxide and difference of surface energies, the size-controlled nanocomposite catalysts may be formed by the MSD system (Fig. 3(h) and (i)) of actual image and schematic diagram of MSD process, respectively).

Fig. 4(a) shows a plot of the current density for methanol electrooxidation with respect to the accelerating potential for PRW-60, PRW-120, and PRW-180. If hydrogen ions produced on the catalyst at the nanocomposite electrode during the oxidation of methanol were transferred on the tungsten oxide, these hydrogen ions would be intercalated into the tungsten oxide. Tungsten oxide is colored when a hydrogen ion is intercalated into the oxide, the so-called cathodic coloration. As shown in Fig. 4(b), variations

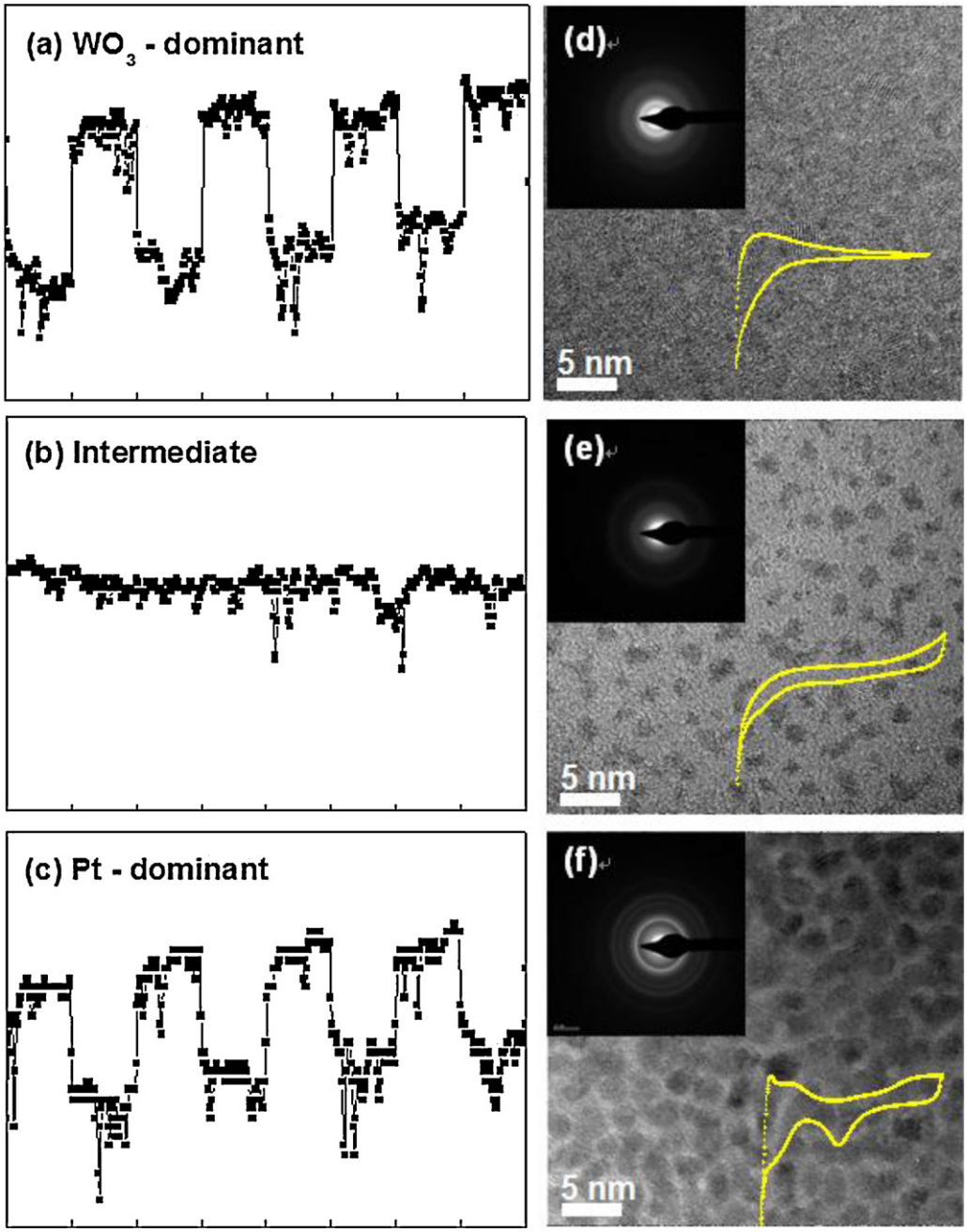

Fig. 5. *In situ* transmittance curves of (a) WO_3-dominant, (b) intermediate-phase, and (c) Pt-dominant catalysts prepared by the MSD system with a pulse potential of −0.3/+0.5 V at an interval of 30 s in 2.0 M CH_3OH + 0.5 M H_2SO_4. TEM images, TED patterns, and *I–V* curves in 0.5 M H_2SO_4 of (d) WO_3-dominant, (e) intermediate-phase, and (f) Pt-dominant catalysts.

in the transmittance in PRW-60, PRW-120, and PRW-180 with respect to an applied potential. The *in situ* photo-electrochemical transmittance measurement for the direct observation of a hydrogen transfer phenomena was carried out using an electrochemical cell for methanol electrooxidation and an optical part consisting of a He–Ne laser (633 nm) as the light source with a power meter for the detection of optical signal modulation (Fig. 4(c)). Hydrogen on the Pt catalyst would be transferred to the WO_3 in the nanostructure catalyst at a positive potential (+0.5 V) and then become colored, resulting in a reduction in the optical signal intensity as the following equation: $Pt—H + WO_x \rightarrow Pt + H—WO_x$. Hydrogen ions produced during methanol oxidation would be transferred to the tungsten oxide in the nanostructure catalyst at +0.5 V of an oxidation potential and would then become colored as a result of the reduced optical signal intensity. The larger reduced intensity of the PRW-120 might result from more hydrogen ions produced by methanol oxidation reaction. Accordingly, we conclude that the PRW-120 with the optimized composition of 62.2 at.% (Pt) and size of 3.62 ± 0.15 nm (PtRu) exhibits an excellent catalytic activity among the electrodes due to size effect of PtRu and spillover effect of WO_3.

As seen in Fig. 5, the variation in transmittance of nanostructure catalysts (WO_3-dominant, intermediate-phase, and Pt-dominant electrode prepared by MSD system) was observed with respect to an applied potential. The optical signal intensity of the WO_3-dominant electrode was reduced (colored) at −0.3 V and

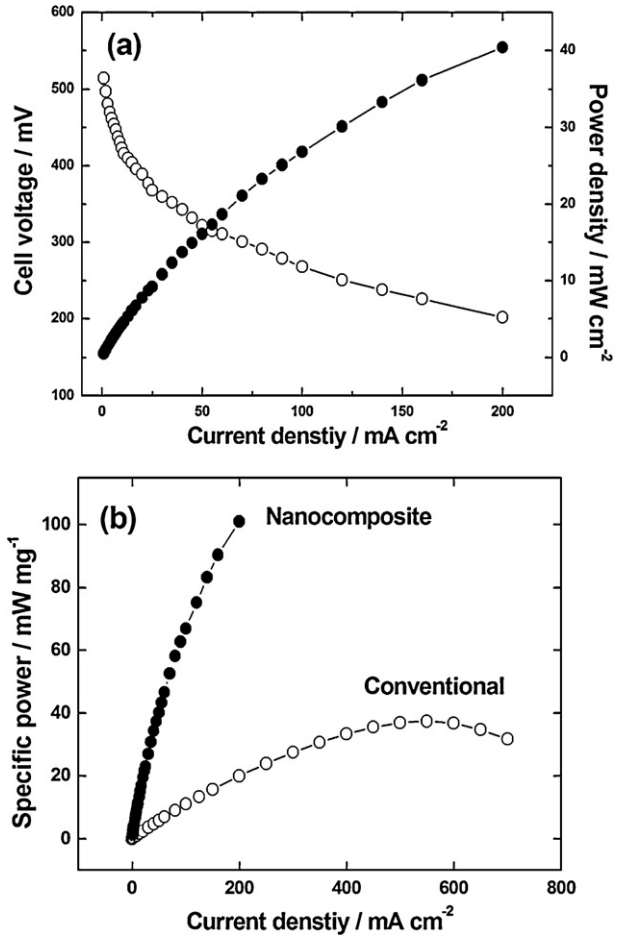

Fig. 6. (a) A characteristic curve of a single cell measured at 25 °C using a nanostructure catalyst (PRW) as an anode and Pt black powder as a cathode. (b) A plot of the specific power ($W\,g^{-1}$) versus current density of the PRW anode catalyst compared to a conventional nanostructure anode catalyst.

increased (bleached) at +0.5 V whereas the intermediate-phase electrode showed no change in intensity with respect to potential. However, it is surprising that the optical signal modulation of the Pt-dominant electrode is exactly the reverse of the WO_3-dominant electrode. This indicates that the hydrogen transfer phenomenon on the WO_3 is affected and modified by the Pt nanophase near the oxide matrix.

A DMFC single cell measurement at 25 °C was carried out using the nanocomposite catalyst as an anode, as shown in the polarization curves (Fig. 6(a)). The open circuit voltage and maximum power density of the DMFC using the nanocomposite catalyst as an anode are ~0.520 V and ~40 $mW\,cm^{-2}$, respectively. Fig. 6(b) shows a plot of the power density per gram of the nanocomposite catalyst compared to a conventional PtRu nanosized catalyst. The mass-normalized power density is one of general evaluation methods to compare the activity of nanostructure catalysts. The mass of the catalyst can be obtained using the following equation: (mass of catalyst) = (growth rate) × (growth time) × (area of electrode) = $(5\,\mu g_{PtRu}\,cm^{-2}\,min^{-1}) \times (2\,min) \times (2\,cm^2) = 20\,\mu g_{PtRu}$. The specific maximum power density of the nanostructure catalyst (~100 $W\,g^{-1}$) is superior to that of the conventional nanostructure catalyst (~37 $W\,g^{-1}$), representing that the nanostructure catalyst has an excellent electrode structure for methanol electrooxidation as compared to the conventional nanostructure catalyst. However, although mass specific power is enhanced, the power density per electrode area the nanostructure catalyst is still low. Accordingly, the MSD process such as porosity control in thickness for the nanocomposite catalysts should be improved for practical applications.

4. Conclusions

We have fabricated nanostructure catalysts for DMFCs by controlling powers of targets in the MSD system. The size and/or composition-controlled nanostructure catalysts showed typical characteristics of Pt or PtRu nanophases and WO_3. The Pt–WO_3 as an anode in the DMFC exhibited improved current density and maximum power density as compared to Pt-only anode. Due to structure and spillover effect, the nanostructure catalyst having PtRu nanophases and WO_3 showed an excellent specific power density as compared to a conventional nanostructure catalyst. It is expected that such nanostructured electrodes will be beneficial to a catalysis study and design of novel electrode structure in fuel cells.

Acknowledgments

This work was supported by the National Research Foundation of Korea Grant funded by the Korean Government (NRF- 2011-0030335) and WCU (World Class University) program through the National Research Foundation of Korea funded by the Ministry of Education, Science and Technology (R31-10013).

References

[1] S. Takaichi, H. Uchida, M. Watanabe, Electrochimica Acta 53 (2008) 4699–4705.
[2] Y.-W. Lee, S.-E. Oh, K.-W. Park, Electrochemistry Communications 13 (2011) 1300–1303.
[3] Y.-W. Lee, A-R. Ko, D.-Y. Kim, S.-B. Han, K.-W. Park, RSC Advances 2 (2012) 1119–1125.
[4] S.H. Ahn, I. Choi, O.J. Kwon, J.J. Kim, Chemical Engineering Journal 181–182 (2012) 276–280.
[5] S. Park, Y. Xie, M.J. Weaver, Langmuir 18 (2002) 5792–5798.
[6] Z. Jusys, J. Kaiser, R.J. Behm, Langmuir 19 (2003) 6759–6769.
[7] L. Chen, G. Lu, Electrochimica Acta 53 (2008) 4316–4323.
[8] C. Wang, H. Daimon, T. Onodera, T. Koda, S. Sun, Angewandte Chemie International Edition 47 (2008) 3588–3591.
[9] J.X. Wang, H. Inada, L. Wu, Y. Zhu, Y. Choi, P. Liu, W.-P. Zhou, R.R. Adzic, Journal of the American Chemical Society 131 (2009) 17298–17302.
[10] E. Reddington, A. Sapienza, B. Gurau, R. Viswanathan, S. Sarangapani, E.S. Smotkin, T.E. Mallouk, Science 280 (1998) 1735–1737.
[11] J.B. Joo, J.S. Kim, P. Kim, J. Yi, Materials Letters 62 (2008) 3497–3499.
[12] H.-S. Oh, H. Kim, Advanced Functional Materials 21 (2011) 3954–3960.
[13] T.-W. Kim, S.-J. Park, L.E. Jones, M.F. Toney, K.-W. Park, Y.-E. Sung, Journal of Physical Chemistry B 109 (2005) 12845–12849.
[14] K.-W. Park, J.-H. Choi, K.-S. Ahn, Y.-E. Sung, Journal of Physical Chemistry B 108 (2004) 5989–5994.
[15] Z. Sun, X. Wang, Z. Liu, H. Zhang, P. Yu, L. Mao, Langmuir 26 (2010) 12383–12389.
[16] V.T.T. Ho, C.-J. Pan, J. Rick, W.-N. Su, B.-J. Hwang, Journal of the American Chemical Society 133 (2011) 11716–11724.
[17] J.-M. Lee, S.-B. Han, J.-Y. Kim, Y.-W. Lee, A-R. Ko, B. Roh, I. Hwang, K.-W. Park, Carbon 48 (2010) 2290–2296.
[18] R. Lv, T. Cui, M.-S. Jun, Q. Zhang, A. Cao, D.S. Su, Z. Zhang, S.-H. Yoon, J. Miyawaki, I. Mochida, F. Kang, Advanced Functional Materials 21 (2011) 999–1006.
[19] L. Vitos, A.V. Ruban, H.L. Skriver, J. Kollár, Surface Science 411 (1998) 186–202.
[20] F.R. de Boer, R. Boom, W.C.M. Mattens, A.R. Miedema, A.K. Niessen, Cohesion in Metals, North-Holland, Amsterdam, 1998.
[21] H. Wang, C. Wingender, H. Baltruschat, M. Lopez, M.T. Reetz, Journal of Electroanalytical Chemistry 509 (2001) 163–169.
[22] H. Wang, T. Loffler, H. Baltruschat, Journal of Applied Electrochemistry 31 (2001) 759–765.
[23] E. Herrero, W. Chrzanowski, A. Wieckowski, Journal of Physical Chemistry 99 (1998) 10423–10424.
[24] Y.-W. Lee, A-R. Ko, S.-B. Han, H.-S. Kim, K.-W. Park, Physical Chemistry Chemical Physics 13 (2011) 5569–5572.
[25] K.-W. Park, J.-H. Choi, B.-K. Kwan, S.-A. Lee, Y.-E. Sung, H.-Y. Ha, S.-A. Hong, H. Kim, A. Wieckowski, Journal of Physical Chemistry B 106 (2002) 1869–1877.
[26] P. Ferrin, M. Mavrikakis, Journal of the American Chemical Society 131 (2009) 14381–14389.
[27] L. Chen, H. Guo, T. Fujita, A. Hirata, W. Zhang, A. Inoue, M. Chen, Advanced Functional Materials 21 (2011) 4364–4370.
[28] Y.-Y. Chu, Z.-B. Wang, Z.-Z. Jiang, D.-M. Gu, G.-P. Yin, Journal of Power Sources 203 (2012) 17–25.

[29] K.-W. Park, Y.-E. Sung, Journal of Physical Chemistry B 109 (2005) 13585–13589.
[30] K. Wang, H.A. Gasteiger, N.M. Markovic, P.N. Ross Jr., Electrochimica Acta 41 (1996) 2587–2593.
[31] B. Moreno, E. Chinarro, J.C. Pérez, J.R. Jurado, Applied Catalysis B: Environmental 76 (2007) 368.
[32] K.-S. Lee, T.-Y. Jeon, S.J. Yoo, I.-S. Park, Y.-H. Cho, S.H. Kang, K.H. Choi, Y.-E. Sung, Applied Catalysis B: Environmental 102 (2012) 334.